ACS APPLIED MATERIALS & INTERFACES

Research Article

www.acsami.org

Subwavelength Gold Grating as Polarizers Integrated with InP-Based InGaAs Sensors

Rui Wang,[†,‡,§] Tao Li,[†,‡] Xiumei Shao,[†,‡] Xue Li,[†,‡] Xiaqi Huang,[∥] Jinhai Shao,[∥] Yifang Chen,*[,∥] and Haimei Gong*[,†,‡]

[†]State Key Laboratories of Transducer Technology, Shanghai Institute of Technical Physics, Chinese Academy of Sciences, Shanghai 200083, People's Republic of China

[‡]Key Laboratory of Infrared Imaging Materials and Detectors, Shanghai Institute of Technical Physics, Chinese Academy of Sciences, Shanghai 200083, People's Republic of China

[§]University of Chinese Academy of Sciences, Beijing 100039, People's Republic of China

[∥]Nanolithography and Application Research Group, State Key Lab of ASIC and System, School of Information Science and Engineering, Fudan University, Shanghai 200433, People's Republic of China

ABSTRACT: There are currently growing needs for polarimetric imaging in infrared wavelengths for broad applications in bioscience, communications and agriculture, etc. Subwavelength metallic gratings are capable of separating transverse magnetic (TM) mode from transverse electric (TE) mode to form polarized light, offering a reliable approach for the detection in polarization way. This work aims to design and fabricate subwavelength gold gratings as polarizers for InP-based InGaAs sensors in 1.0−1.6 μm. The polarization capability of gold gratings on InP substrate with pitches in the range of 200−1200 nm (fixed duty cycle of 0.5) has been systematically studied by both theoretical modeling with a finite-difference time-domain (FDTD) simulator and spectral measurements. Gratings with 200 nm lines/space in 100-nm-thick gold have been fabricated by electron beam lithography (EBL). It was found that subwavelength gold gratings directly integrated on InP cannot be applied as good polarizers, because of the existence of SPP modes in the detection wavelengths. An effective solution has been found by sandwiching the Au/InP bilayer using a 200 nm SiO_2 layer, leading to significant improvement in both TM transmission and extinction ratio. At 1.35 μm, the improvement factors are 8 and 10, respectively. Therefore, it is concluded that the Au/SiO_2/InP trilayer should be a promising candidate of near-infrared polarizers for the InP-based InGaAs sensors.

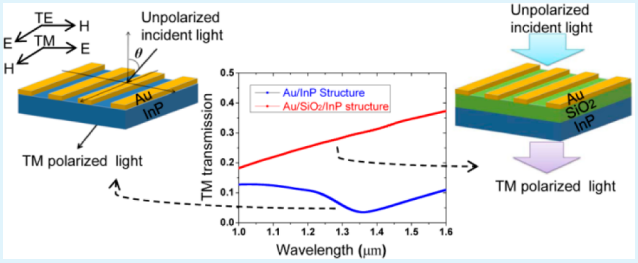

KEYWORDS: *subwavelength gold grating, polarizer, surface plasmon polariton, cavity mode, InP-based InGaAs sensor*

1. INTRODUCTION

The polarimetric imaging technique provides unique advantages in the detection of images with improved contrast and low noise over conventional wavelength ones. Because of this, it has exhibited extensive applications. Notably, in medicine, it can be applied to enhance the contrast between healthy and cancerous zones of colon specimens, in order to facilitate the early detection of cancer.[1] In environmental protection, it can spot oil-slick-contaminated sea surfaces in slick-free areas.[2] In biological systems, it was used in mantis shrimp compound eyes to improve underwater sensitivity.[3] In forensic science, it can improve the efficiency to detect latent fingerprint images.[4] Traditionally, polarization information is obtained by rotating a linear polarizer in front of the sensor.[5,6] Stokes parameters are captured at different instants of time, leading to the artifacts in polarimetric imaging, especially for fast moving targets.[7] To eliminate these defects, division of focal plane (DoFP) is introduced by monolithically integrating pixelated micropolarizers of different orientations onto the sensor, to obtain instantaneous Stokes parameters.[8−10]

It has been well-known that a subwavelength metallic grating (SMG) has the function of polarization, in which transverse magnetic (TM) mode is transmitted and transverse electric (TE) mode is blocked for a light impinging onto it.[11−17] Compared with crystal and polymer polarizer, SMG has the advantages of miniaturized dimensions, high spatial resolution, and good temperature tolerance, which is beneficial for highly pixelated match requirement in DoFP polarimetric imaging.[18] InGaAs material with lattice matched InP substrate has been widely used in the field of astronomical detection, Earth observation, and machine vision.[19−21] SMG has been integrated onto CCD/CMOS to prove the feasibility in the visible range.[18,22−24] However, the integration of SMG onto short-wave infrared (SWIR) InGaAs sensor has yet been reported so far.

Received: April 28, 2015
Accepted: June 17, 2015
Published: June 26, 2015

DOI: 10.1021/acsami.5b03679
ACS Appl. Mater. Interfaces 2015, 7, 14471−14476

In this work, we proposed to integrate a subwavelength gold grating (SGG) as a polarizer to InP-based InGaAs sensors for the application in polarization detection in 1.0−1.6 μm. However, it was discovered that SGG with a pitch of 200−500 nm cannot fully functionalize as a polarizer, because of the existence of SPP resonance. This problem was successfully solved by inserting a 200 nm SiO_2 layer into the Au/InP interface. Nanofabrication of SGG polarizers was fabricated by electron beam lithography (EBL). The polarization property of the fabricated SGG has been carefully characterized by both numerical simulation and optical measurements, demonstrating its promising future in the application of InP-based InGaAs detector for polarimetric imaging.

2. EXPERIMENTAL SECTION

Fabrication of SGG Polarizers. For comparison, 200 nm lines/space gold gratings were fabricated on InP and SiO_2/InP, respectively, by EBL, followed by gold thermal deposition and lift-off in acetone. The grating area is 2 mm × 2 mm, and the gold thickness is 100 nm. In the EBL, a positive tone UVIII was first spin-coated on InP substrate at 4000 rpm for 60 s for a thickness of ~600 nm, then baked at 130 °C for 60 s immediately. A state-of-the-art beam writer (Model JBX-6300FS, JEOL) was used for e-beam exposure, followed by post-exposure bake at 130 °C for 90 s. The exposed resist was subsequently developed by CD26 at 23 °C for 60 s, and finally rinsed in deionized water (DIW) for 30 s. On this basis, 10 nm Cr/100 nm gold was deposited using thermal evaporation with NANO36 (Kurt J. Lesker). The process was completed by a lift-off in acetone. Figure 1 presents a micrograph by scanning electron microscopy (SEM) for the fabricated gold grating.

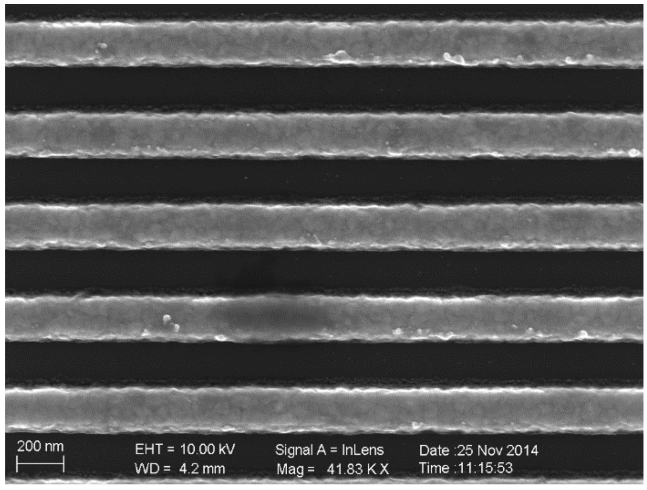

Figure 1. A SEM micrograph for the fabricated subwavelength gold grating (SGG) on a InP substrate.

Optical Measurement. Two optical systems, as schematically shown in Figure 2, were built to measure the transmission of SGG polarizers. For the measurement of normal transmission spectrum in the range of 1.0−1.6 μm, a tungsten-halogen lamp was used (Figure 2a). After passing through a commercial polarizer, the sample, and a grating spectrometer in sequence, the emergent light was received by an InGaAs sensor. For angle-resolved transmission spectra, a solid-state laser (wavelength = 1342 nm, beam diameter = 1.5 mm) was used as a light source, followed by a neutral density filter, a quarter-wave plate, and a Glan-Thompson polarizer (Figure 2b). The laser beam was confined by using a 1 mm × 1 mm diaphragm. Both the sample and the diaphragm were fixed on a rotational stage by which the incident angle was changed in the range of 0−35°. All measurements were carried out at room temperature. The measured data were smoothed by fast Fourier transform (FFT).

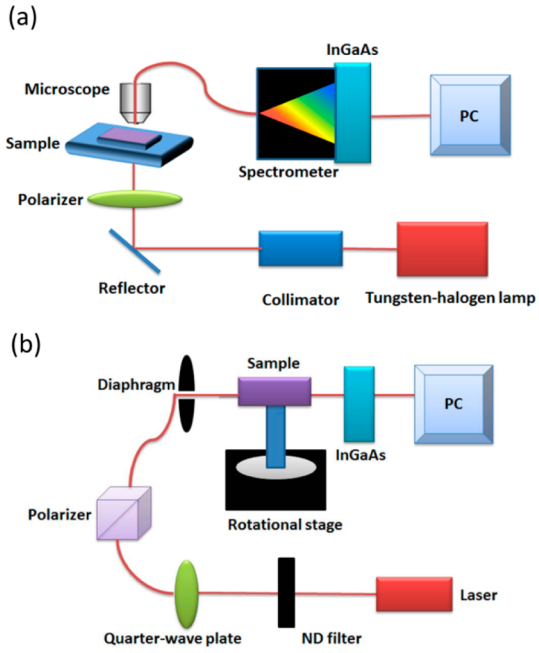

Figure 2. Schematics of optical measurement systems: (a) normal transmission spectrum in the range of 1.0−1.6 μm and (b) angle-resolved transmission spectrum at 1342 nm.

3. RESULTS AND DISCUSSION

In this section, polarization property of SGG on InP and SiO_2/InP, respectively, are investigated by both theoretically modeling and optical measurement.

SGG Polarizer on InP. The transmission spectra of SGG on InP were first calculated using the FDTD algorithm[25] with commercial software delivered by Lumerical, Ltd. To gain insight of the transmission mechanism, electric field distributions and the Poynting vector were also computed. The frequency-dependent dielectric constant functions of gold and InP were fitted by multicoefficient models (MCMs).[26] The dielectric constant of SiO_2 was taken to be 2.09. Periodic boundary condition (under normal incidence) or Bloch boundary condition (under oblique incidence) were used in the SGG plane, and perfectly matched layer (PML) boundary condition was chosen normal to the SGG plane. A linear-polarized plane wave in the range of 1.0−1.6 μm was selected as the light source.

Figure 3 shows the simulated transmission spectra and extinction ratio of SGG polarizer fabricated on InP, as a function of wavelength and pitch. When the pitch is larger than 500 nm, TE transmission (Figure 3b) is just over 20%, indicating a poor polarization performance. Although TE transmission is suppressed for the pitches below 500 nm (Figure 3b), a low TM transmission in the same area (Figure 3a) is also observed in the range of 1.0−1.6 μm, resulting in low extinction ratio in Figure 3c.

It is understood that the dark area in Figure 3a is caused by propagating surface plasmonic polariton (SPP). As a SPP wave propagates at the interface, wave vector conservation is provided by diffraction on a periodic structure.[27]

DOI: 10.1021/acsami.5b03679
ACS Appl. Mater. Interfaces 2015, 7, 14471−14476

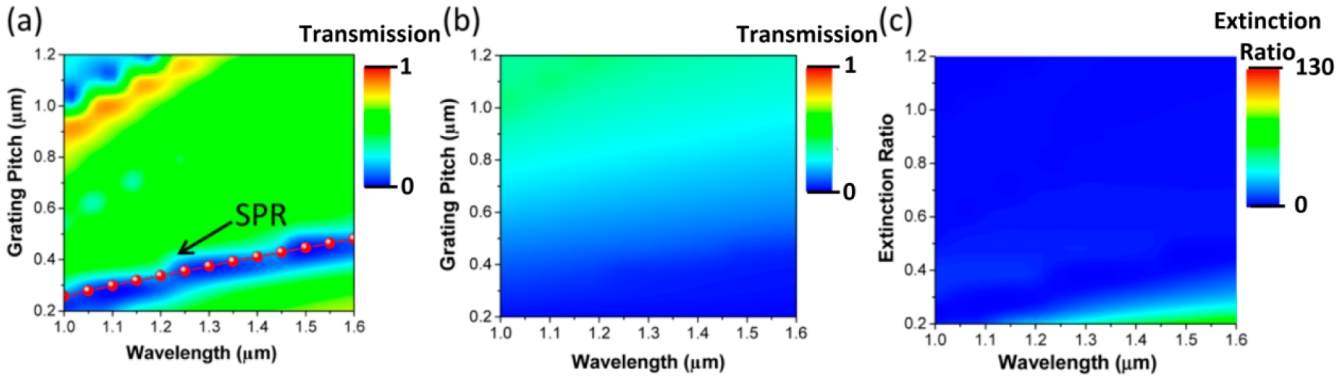

Figure 3. Simulated normal incident transmission spectra of Au/InP structure, as a function of wavelength and pitch: (a) TM polarized incident light, (b) TE polarized incident light, and (c) extinction ratio, as defined by TM/TE. The red dotted line in panel a presents the SPP resonance ($i = \pm 1$, $j = 0$) in the Au/InP interface.

$$\mathbf{k}_{SP} = \mathbf{k}_0 \sin\theta \pm i\left(\frac{2\pi}{D_x}\right)\mathbf{u}_x \pm j\left(\frac{2\pi}{D_y}\right)\mathbf{u}_y \quad (1)$$

where $\mathbf{K}_{sp}$ is the SP wavevector, $\mathbf{K}_0$ is the wavevector of light in vaccine, θ is the angle of incidence, $D_{x,y}$ is the periodicity of the structured film in the x- and y-directions, $\mathbf{u}_x$ and $\mathbf{u}_y$ are the reciprocal lattice vector, and i and j are integer numbers corresponding to different directions of SPP. In addition, the magnitude of SP wave vector is given by

$$|\mathbf{K}_{SP}| = \frac{2\pi}{\lambda}\sqrt{\frac{\varepsilon_m\varepsilon_d}{\varepsilon_m + \varepsilon_d}} \quad (2)$$

where λ is the wavelength of incident light, ε_m the permittivity of metal, and ε_d the permittivity of the adjacent medium.

For normal incidence of light onto an SGG, using eqs 1 and 2, the SPP resonance wavelength is obtained:

$$\lambda_{SPP} = \frac{D}{\sqrt{i^2 + j^2}}\sqrt{\frac{\varepsilon_m\varepsilon_d}{\varepsilon_m + \varepsilon_d}} \quad (3)$$

which depicts the relationship between the SPP wavelength (λ_{SPP}) and the grating pitch (D) in the Au/InP interface for $i = \pm 1$, $j = 0$, as shown by the red dotted line in Figure 3a, proving that the dark area is truly caused by SPP resonance. Figure 4 presents simulated and measured transmission spectra in the range of 1.0−1.6 μm for a fixed pitch of 400 nm, both of which show that the light in the 1.3−1.44 μm range is not polarized.

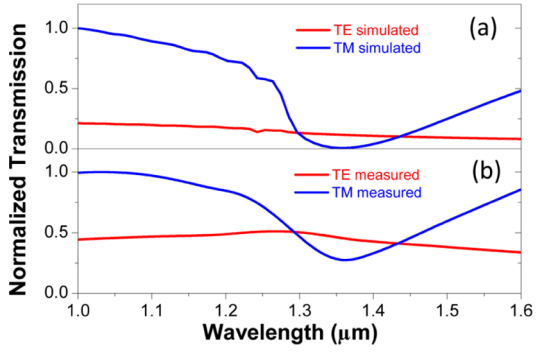

Figure 4. Simulated and measured transmission spectra of Au/InP structure with pitch = 400 nm, gold thickness = 100 nm, and duty cycle = 0.5: (a) simulated transmission spectra and (b) measured transmission spectra.

Some deviations between measured and calculated value may be ascribed to the specific geometric parameters of the fabricated SGG polarizer.

Figure 5 presents both the simulated and measured transmission with different incidence angles at 1342 nm,

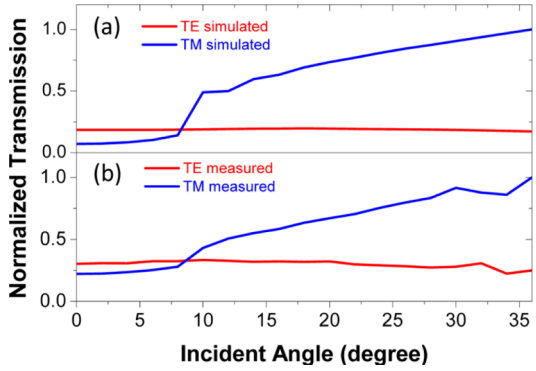

Figure 5. Simulated and measured angle-resolved transmission spectra of Au/InP structure for the wavelength at 1342 nm: (a) simulated transmission spectra and (b) measured transmission spectra.

which is close to the minimum of TM transmission. Both theoretical and experimental transmittances show unpolarization behavior for the angle between ±8°. According to eq 1, the SPP excitation is strongly related to the incident angle θ. With the increasing of incident angle, SPP resonance disappears, leading to the increase of TM transmission. Although polarization begins to play with larger oblique incidence angles, the incident light intensity decreases, resulting in low detection efficiency.

Figure 6 presents the electric field distribution and Poynting vectors of TM mode with normal incidence (Figure 6a), as well as oblique incidence at 30° (Figure 6b) at 1.35 μm. For normal incidence, a strong reflection of light can be clearly seen in the E^2 distribution, stemming from SPP mode, as discussed above. This is consistent with the power flow described by the simulated Poynting vector distribution in Figure 6a (i.e., negligible power flows through the InP substrate). However, for the oblique incidence in Figure 6b, SPP resonance disappears, leading to nonzero power flow into InP.

The existence of unpolarized area due to SPP mode in the concerned wavelengths significantly impairs the extinction quality of our polarizers. In order to eliminate the unwanted SPP modes in 1.0−1.6 μm with an SGG as a polarizer on InP, a

DOI: 10.1021/acsami.5b03679
ACS Appl. Mater. Interfaces 2015, 7, 14471−14476

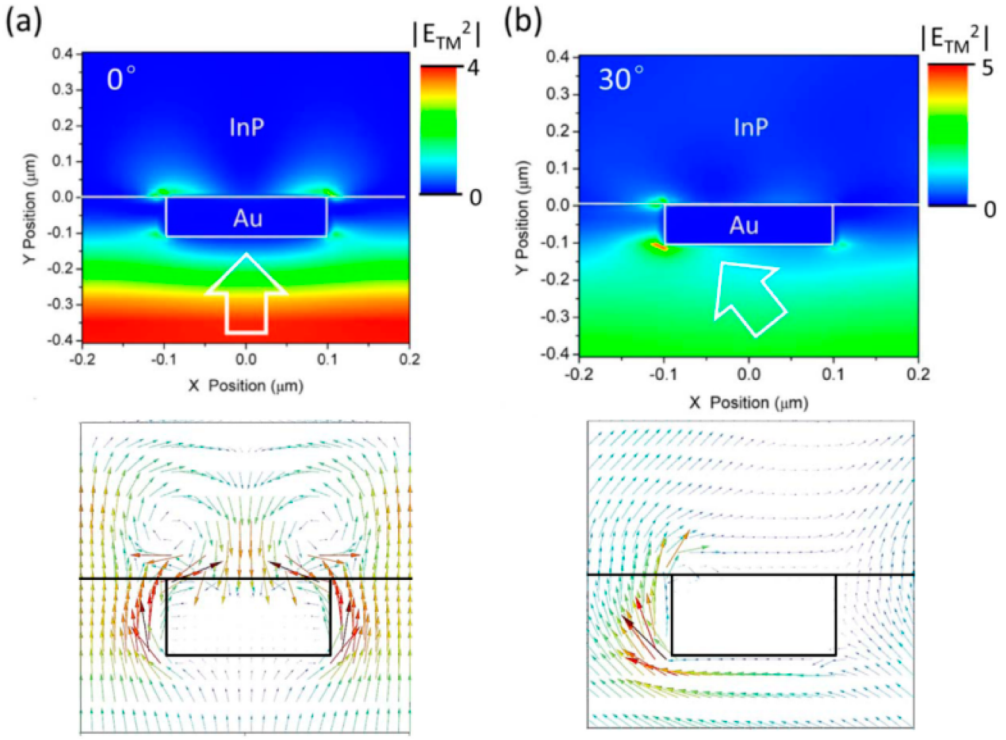

Figure 6. Electric field distributions and Poynting vectors of TM mode in Au/InP structure at 1350 nm wavelength: (a) incident angle = 0° and (b) incident angle = 30°.

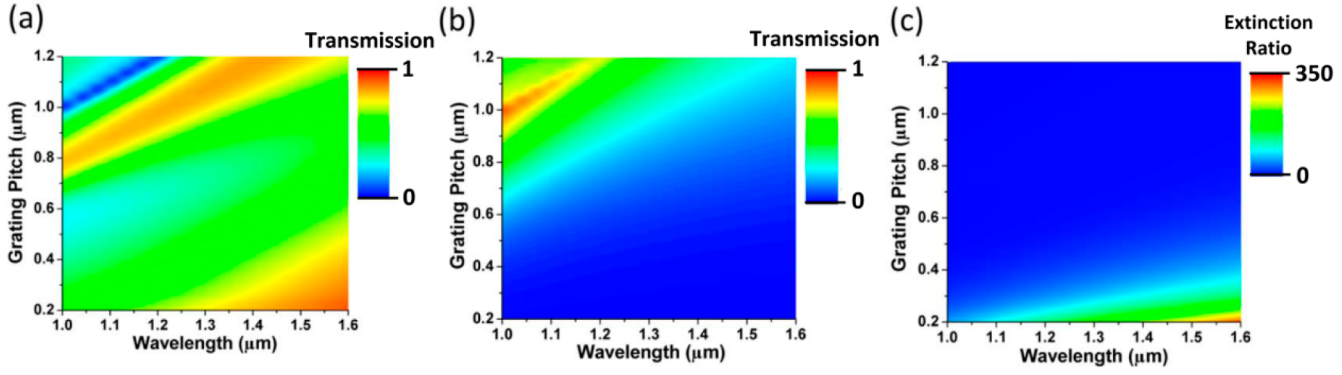

Figure 7. Simulated normal incident transmission spectra of Au/SiO_2/InP structure, as a function of wavelength and pitch: (a) TM polarized incident light, (b) TE polarized incident light, and (c) extinction ratio, as defined by TM/TE.

dielectric layer with lower permittivity ε_d should be plugged into the interface between gold and InP (eq 2). In this work, a 200 nm SiO_2 film with ε_d = 2.09 is selected. Such a SiO_2 layer not only moves the SPP mode out of the 1.0−1.6 μm, but also acts as an antireflection layer, as will be discussed later.

SGG Polarizer on SiO_2/InP. As mentioned above, an efficient way to eliminate the SPP mode in the sensing region of 1.0−1.6 μm is to add a SiO_2 layer between gold and InP to form a Au/SiO_2/InP sandwich structure. Figure 7 presents the transmission and extinction ratios of a Au/SiO_2/InP structure with a SiO_2 thickness of 200 nm. The dark area in TM transmission has disappeared (Figure 7a) and lower TE transmission is presented (Figure 7b), resulting in significantly improved polarization performance over the Au/InP structure (Figure 7c).

Figure 8 presents both the simulated and measured TM mode transmission for a specific grating pitch of 400 nm. Clear polarization is observed in the entire region of 1.0−1.6 μm. The

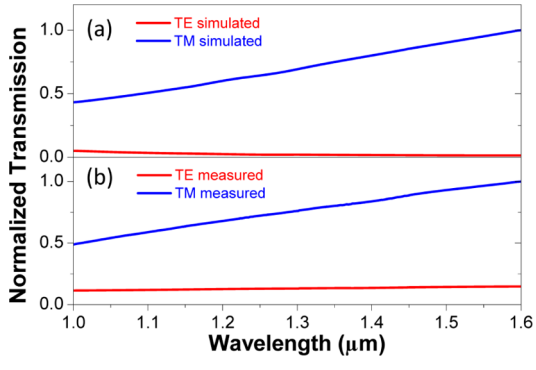

Figure 8. Simulated and measured transmission spectra of a Au/SiO_2/InP structure with pitch = 400 nm, SiO_2 thickness = 200 nm, and duty cycle = 0.5: (a) simulated transmission spectra and (b) measured transmission spectra. The TM transmission dip at 1350 nm is totally removed.

DOI: 10.1021/acsami.5b03679
ACS Appl. Mater. Interfaces 2015, 7, 14471−14476

simulated transmittance is quantitatively in good agreement with the measured value, indicating that the SiO_2 in the Au/InP interface is essential for the SGG to be a polarizer on the InP substrate.

With such an SGG/SiO_2/InP trilayer, the permittivity of the media around the gold grating is changed from 10.2 (InP at 1350 nm) to 2.1 (SiO_2), shifting the resonance wavelength from 1350 nm to 650 nm (see eq 2). Moreover, the SiO_2 layer can play a role of an antireflection layer to improve the quantum efficiency of the InGaAs sensor. Therefore, the Au/SiO_2/InP structure should be a reasonable choice for the polarizer in InP-based InGaAs sensors in the range of 1.0−1.6 μm.

To further study the transmission process of TM mode, both the electric field distribution and Poynting vectors were calculated for the Au/SiO_2/InP structure, as shown in Figure 9. Poynting vector plot also illustrates enhanced power flow

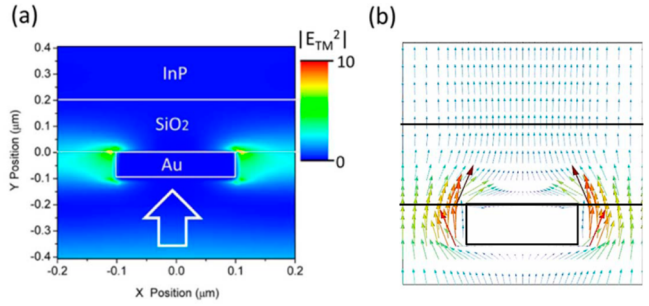

Figure 9. TM mode in a Au/SiO_2/InP structure at 1350 nm: (a) electric field distribution and (b) Poynting vector distribution.

into the InP substrate. In our case, there are two types of resonance mechanisms: (i) SPP resonance (horizontal surface-plasmon resonance) in the Au/InP interface, and (ii) localized cavity mode (vertical surface-plasmon resonance) located in the slits.[28,29] In the Au/InP structure, SPP resonance is the dominant mechanism. The horizontal SPP reduces the transmission, as shown in Figure 3, by either reflecting some of the light or converting into Joule loss in the substrate. By adding a layer of SiO_2 to the interface of Au/InP, the horizontal SPP is eliminated, to reduce the reflectance. Consequently, the transmission is increased via the localized cavity mode, as shown by the very strong electric field and Poynting vectors in the slits in Figure 9.

Furthermore, the thickness of SiO_2 should be carefully selected to maximize the transmission. Figure 10 presents the calculated TM transmission at various SiO_2 thicknesses from 100 nm to 600 nm. It can be seen that the transmission can vary by 40% at 1.35 μm for different thicknesses. Using the transmission result in Figure 10 as a guide, the thickness of SiO_2 should be designed according to the specific working wavelengths of the InGaAs sensor. Particularly for the interested wavelength of 1.35 μm, a thickness of 100 nm should be used.

4. CONCLUSION

This paper investigates the feasibility of subwavelength metallic gratings as polarizers in short-wave infrared wavelengths for InP-based InGaAs sensors. Au/InP and Au/SiO_2/InP structures were compared by FDTD simulation and optical characterizations. The Au/InP structure shows a large TM transmittance dip with no polarization for the grating pitch

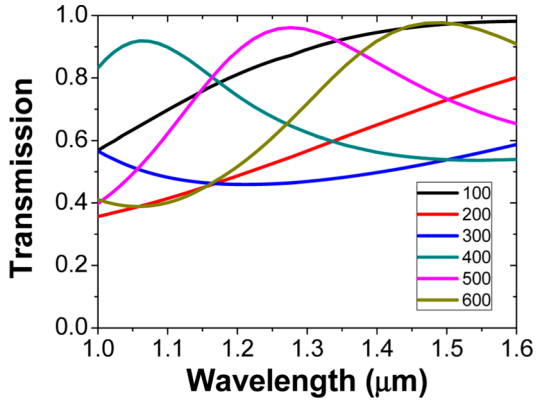

Figure 10. Calculated TM transmission spectra of the Au/SiO_2/InP structure as a function of SiO_2 thickness in the range of 100−600 nm.

from 200 nm to 500 nm. The low TM transmission in this structure has been explained by the existence of SPP resonance in the Au/InP interface. However, the Au/SiO_2/InP structure has demonstrated a stable TM transmission and extinction ratio in the entire sensing wavelength. Polarizers with such a sandwich structure have been successfully fabricated and its polarization capability has been demonstrated by optical characterization. Besides, the added SiO_2 layer should be beneficial to the transmission improvement as an antireflection layer. This work sheds lights on further development of integrated polarimetric sensors in short-wave infrared region. Further work in the selection of metal materials, as well as optimization of the pitch and duty cycle, should be carried out for improving the polarization performance.

AUTHOR INFORMATION

Corresponding Authors

*E-mail: yifangchen@fudan.edu.cn (Y. Chen).
*E-mail: hmgong@mail.sitp.ac.cn (H. Gong).

Author Contributions

The manuscript was written through contributions of all authors. All authors have given approval to the final version of the manuscript.

Notes

The authors declare no competing financial interest.

ACKNOWLEDGMENTS

This project is supported by the National Key Basic Research and Development Program of China (973 Program No. 2012CB619200) and National Natural Science Foundation of China (Nos. 61205105, 61376052, and 61475179).

REFERENCES

(1) Novikova, T.; Pierangelo, A.; Manhas, S.; Benali, A.; Validire, P.; Gayet, B.; De Martino, A. The Origins of Polarimetric Image Contrast between Healthy and Cancerous Human Colon Tissue. *Appl. Phys. Lett.* **2013**, *102*, 241103.

(2) Zhang, B.; Perrie, W.; Li, X.; Pichel, W. G. Mapping Sea Surface Oil Slicks Using RADARSAT-2 Quad-Polarization SAR Image. *Geophys. Res. Lett.* **2011**, 38.

(3) Cronin, T. W.; Marshall, J. Parallel Processing and Image Analysis in the Eyes of Mantis Shrimps. *Biol. Bull.* **2001**, *200*, 177−183.

(4) Lin, S. S.; Yemelyanov, K. M.; Pugh, E. N.; Engheta, N. Polarization-Based and Specular-Reflection-Based Noncontact Latent Fingerprint Imaging and Lifting. *J. Opt. Soc. Am. A* **2006**, *23*, 2137−2153.

DOI: 10.1021/acsami.5b03679
ACS Appl. Mater. Interfaces 2015, 7, 14471−14476

(5) Goldstein, D. H. Mueller Matrix Dual-Rotating Retarder Polarimeter. *Appl. Opt.* **1992**, *31*, 6676−6683.
(6) Egan, W. G.; Johnson, W. R.; Whitehead, V. S. Terrestrial Polarization Imagery Obtained from the Space Shuttle: Characterization and Interpretation. *Appl. Opt.* **1991**, *30*, 435−442.
(7) Marconnet, P.; Gendre, L.; Foulonneau, A.; Bigue, L. Cancellation of Motion Artifacts Caused by a Division-of-Time Polarimeter. *Proc. SPIE* **2011**, *8160*, 81600M.
(8) Perkins, R.; Gruev, V. Signal-to-Noise Analysis of Stokes Parameters in Division of Focal Plane Polarimeters. *Opt. Express* **2010**, *18*, 25815−25824.
(9) Myhre, G.; Hsu, W. L.; Peinado, A. Liquid Crystal Polymer Full-Stokes Division of Focal Plane Polarimeter. *Opt. Express* **2012**, *20*, 27393−27409.
(10) Tyo, J. S. Hybrid Division of Aperture/Division of a Focal-Plane Polarimeter for Real-Time Polarization Imagery without an Instantaneous Field-of-View Error. *Opt. Lett.* **2006**, *31*, 2984−2986.
(11) Hall, A. S.; Faryad, M.; Barber, G. D.; Liu, L.; Erten, S.; Mayer, T. S.; Lakhtakia, A.; Mallouk, T. E. Broadband Light Absorption with Multiple Surface Plasmon Polariton Waves Excited at the Interface of a Metallic Grating and Photonic Crystal. *ACS Nano* **2013**, *7*, 4995−5007.
(12) Schider, G.; Krenn, J. R.; Gotschy, W.; Lamprecht, B.; Ditlbacher, H.; Leitner, A.; Aussenegg, F. R. Optical Properties of Ag and Au Nanowire Gratings. *J. Appl. Phys.* **2001**, *90*, 3825−3830.
(13) Asano, K.; Yokoyama, S.; Kemmochi, A.; Yatagai, T. Fabrication and Characterization of a Deep Ultraviolet Wire Grid Polarizer with a Chromium-Oxide Subwavelength Grating. *Appl. Opt.* **2014**, *53*, 2942−2948.
(14) Gao, S.; Njuguna, R.; Gruev, V. Fabrication and Performance Evaluation of Pixelated Nano-Wire Grid Polarizer. *Proc. SPIE* **2013**, *8873*, 88730L.
(15) Takano, K.; Yokoyama, H.; Ichii, A.; Morimoto, I.; Hangyo, M. Wire-Grid Polarizer Sheet in the Terahertz Region Fabricated by Nanoimprint Technology. *Opt. Lett.* **2011**, *36*, 2665−2667.
(16) Shishido, S.; Noda, T.; Sasagawa, K.; Tokuda, T.; Ohta, J. Polarization Analyzing Image Sensor with On-Chip Metal Wire Grid Polarizer in 65-nm Standard Complementary Metal Oxide Semiconductor Process. *Jpn. J. Appl. Phys.* **2011**, *50*, 04DL01.
(17) Cetnar, J. S.; Middendorf, J. R.; Brown, E. R. Extraordinary Optical Transmission and Extinction in a Terahertz Wire-Grid Polarizer. *Appl. Phys. Lett.* **2012**, *100*, 231912.
(18) Gruev, V.; Perkins, R.; York, T. CCD Polarization Imaging Sensor with Aluminum Nanowire Optical Filters. *Opt. Express* **2010**, *18*, 19087−19094.
(19) Hoogeveen, R. W. M.; Goede, A. P. H. Extended Wavelength InGaAs Infrared (1.0−2.4 μm) Detector Arrays on SCIAMACHY for Space-Based Spectrometry of the Earth Atmosphere. *Infrared Phys. Technol.* **2001**, *42*, 1−16.
(20) MacDougal, M.; Geske, J.; Wang, C.; Shirong, L.; Getty, J.; Holmes, A. Low Dark Current InGaAs Detector Arrays for Night Vision and Astronomy. *Proc. SPIE* **2009**, *7298*, 72983F.
(21) Shao, X. M.; Zhu, Y. M.; Li, X.; Tang, H. J.; Li, T.; Gong, H. M. The Influence of Sunlight Irradiation on the Characteristics of InGaAs Detectors. *Proc. SPIE* **2014**, *9220*, 92200A.
(22) Tokuda, T.; Sato, S.; Yamada, H.; Sasagawa, K.; Ohta, J. Polarisation-Analysing CMOS Photosensor with Monolithically Embedded Wire Grid Polariser. *Electron. Lett.* **2009**, *45*, 228−229.
(23) Sarkar, M.; Bello, D. S. S.; van Hoof, C.; Theuwissen, A. Integrated Polarization Analyzing CMOS Image Sensor for Material Classification. *IEEE Sens. J.* **2011**, *11*, 1692−1703.
(24) Guillaumee, M.; Dunbar, L. A.; Santschi, C.; Grenet, E.; Eckert, R.; Martin, O. J. F.; Stanley, R. P. Polarization Sensitive Silicon Photodiodes Using Nanostructured Metallic Grids. *Appl. Phys. Lett.* **2009**, *94*, 193503.
(25) Kunz, K. S.; Luebbers, R. J. *The Finite Difference Time Domain Method for Electromagnetics*; CRC Press: Boca Raton, FL, 1993.
(26) Palik, E. D. *Handbook of Optical Constants of Solids*; Academic Press: New York, 1998.
(27) Raether, H. *Surface Plasmons on Smooth Surfaces*; Springer: Berlin, Heidelberg, Germany, 1988.
(28) Collin, S.; Pardo, F.; Teissier, R.; Pelouard, J. L. Strong Discontinuities in the Complex Photonic Band Structure of Transmission Metallic Gratings. *Phys. Rev. B* **2001**, *63*, 033107.
(29) Garcia-Vidal, F. J.; Martin-Moreno, L. Transmission and Focusing of Light in One-Dimensional Periodically Nanostructured Metals. *Phys. Rev. B* **2002**, *66*, 155412.

DOI: 10.1021/acsami.5b03679
ACS Appl. Mater. Interfaces 2015, 7, 14471−14476